# Nanospherical arabinogalactan proteins are a key component of the high-strength adhesive secreted by English ivy

Yujian Huang[a,b,c], Yongzhong Wang[a,b,c], Li Tan[d,e], Leming Sun[a,b,c], Jennifer Petrosino[c], Mei-Zhen Cui[f], Feng Hao[f], and Mingjun Zhang[a,b,c,1]

[a]Department of Biomedical Engineering, College of Engineering, The Ohio State University, Columbus, OH 43210; [b]Interdisciplinary Biophysics Graduate Program, The Ohio State University, Columbus, OH 43210; [c]Dorothy M. Davis Heart & Lung Research Institute, The Ohio State University Wexner Medical Center, Columbus, OH 43210; [d]Complex Carbohydrate Research Center, University of Georgia, Athens, GA 30602; [e]DOE BioEnergy Science Center, University of Georgia, Athens, GA 30602; and [f]Department of Biomedical and Diagnostic Sciences, College of Veterinary Medicine, University of Tennessee, Knoxville, TN 37996

Over 130 y have passed since Charles Darwin first discovered that the adventitious roots of English ivy (*Hedera helix*) exude a yellowish mucilage that promotes the capacity of this plant to climb vertical surfaces. Unfortunately, little progress has been made in elucidating the adhesion mechanisms underlying this high-strength adhesive. In the previous studies, spherical nanoparticles were observed in the viscous exudate. Here we show that these nanoparticles are predominantly composed of arabinogalactan proteins (AGPs), a superfamily of hydroxyproline-rich glycoproteins present in the extracellular spaces of plant cells. The spheroidal shape of the AGP-rich ivy nanoparticles results in a low viscosity of the ivy adhesive, and thus a favorable wetting behavior on the surface of substrates. Meanwhile, calcium-driven electrostatic interactions among carboxyl groups of the AGPs and the pectic acids give rise to the cross-linking of the exuded adhesive substances, favor subsequent curing (hardening) via formation of an adhesive film, and eventually promote the generation of mechanical interlocking between the adventitious roots of English ivy and the surface of substrates. Inspired by these molecular events, a reconstructed ivy-mimetic adhesive composite was developed by integrating purified AGP-rich ivy nanoparticles with pectic polysaccharides and calcium ions. Information gained from the subsequent tensile tests, in turn, substantiated the proposed adhesion mechanisms underlying the ivy-derived adhesive. Given that AGPs and pectic polysaccharides are also observed in bioadhesives exuded by other climbing plants, the adhesion mechanisms revealed by English ivy may forward the progress toward understanding the general principles underlying diverse botanic adhesives.

ivy nanoparticle | ivy adhesive | arabinogalactan protein | adhesion mechanism | reconstructed adhesive

Although there is a growing interest in exploring mechanisms regulating a variety of adhesive behaviors in the animal kingdom (1–6), the molecular basis allowing creeping plants, such as English ivy (*Hedera helix*), to generate sufficient adhesive force, aiding in clinging to vertical surfaces, is rarely discussed (Fig. 1*A*). Previous studies have emphasized mechanical strategies exploited by multiple climbing organs that evolve in plants (7–11). Nevertheless, the role of the glue-like viscous exudates that are observed on the majority of these organs and that cement the plants to the substrates has been less explored (10, 12, 13). Diverse polysaccharides and glycoproteins, comprising mucilaginous pectins, arabinogalactans, arabinogalactan proteins (AGPs), and many others, have been identified to be the predominant components in these adhesive substances (14–17); however, the molecular mechanisms underlying the high-strength adhesion remain elusive.

By means of atomic force microscopy (AFM), bulk spherical organic nanoparticles have been observed in the exudates derived from the root hairs of English ivy (18–20). These proteinaceous nanoparticles are presumed to exert crucial roles in facilitating the attachment of the adventitious roots and favoring the climbing of English ivy (21). However, the exact chemical constitution of the ivy nanoparticles has not been identified.

Herein, we report that the ivy nanoparticles are predominantly composed of AGPs. Via further exploring physicochemical cues that are potentially associated with the generation of strong adhesion strength, the roles of these AGP-rich nanoparticles in the high-strength adhesive are elucidated. Inspired by the molecular basis controlling the adhesive action, a reconstructed biomimetic adhesive was subsequently developed. This ivy-mimetic adhesive not only serves as an instance to support the proposed molecular basis for the ivy adhesive but also offers a promising template for guiding the development of ivy-derived and ivy-inspired high-strength adhesive materials.

## Results

**Ivy Nanoparticles Inherit the Tertiary Structure of the AGPs.** A platform for cost-effective cultivation of *H. helix* has been developed previously (22, 23). This in vitro cultivation system not only raises the yield of the adventitious roots and the ivy nanoparticles (22) but

### Significance

Despite the significant progress that has been made in exploring the molecular basis for multiple adhesive events in the animal kingdom, the exceptional adhesion behaviors of climbing plants, such as English ivy, are still poorly understood. In this study, the spheroidal nanoparticles observed in the mucilage exuded by the English ivy were identified to be predominantly composed of arabinogalactan proteins (AGPs). The roles of these AGP-rich nanoparticles in favoring the generation of strong adhesion strength are elucidated. The $Ca^{2+}$-driven electrostatic interactions among uronic acids within AGPs and pectin upon curing could be exploited as guidelines in the design and fabrication of novel synthetic adhesives, and the ivy-derived adhesive composite is capable of serving as a template for inspiring the development of diverse adhesive biomaterials.
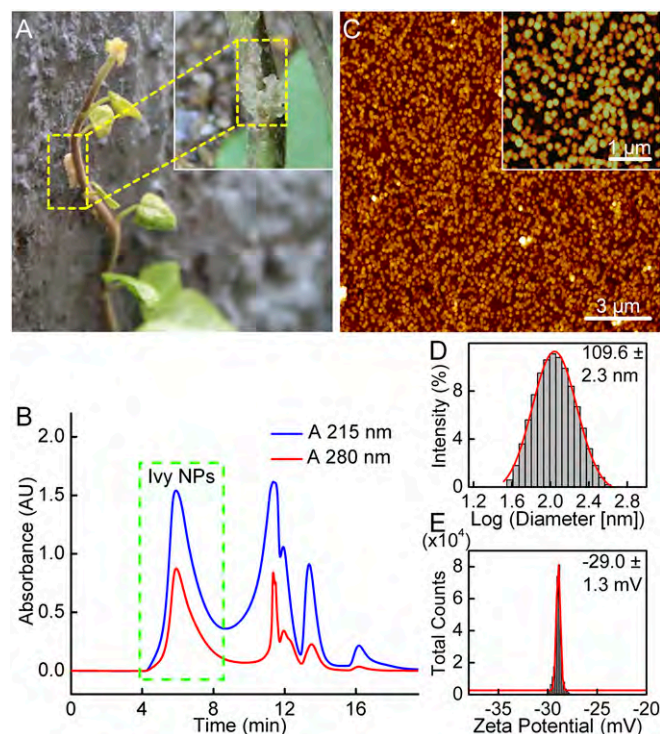
**Fig. 1.** Characterization of the nanoparticles isolated from the adventitious roots of English ivy. (*A*) Ivy shoots attached to the wall. Rich adventitious roots observed in the area circled in yellow. (*Inset*) Adhesive pads formed by the adventitious roots. (*B*) SEC profiles of the root extracts prepared by sonication and filtration. The UV absorbance of the eluent was monitored at 215 nm and 280 nm, simultaneously. The first major fraction was collected and lyophilized for microscopic examination and further chemical identification. (*C*) AFM images of the purified ivy nanoparticles with an average diameter of ∼70 nm. (*Inset*) High-magnification view. (Scale bars, 3 μm and 1 μm, respectively.) (*D*) Size distribution of the purified ivy nanoparticles, with an average hydrodynamic size of 109.6 ± 2.3 nm in diameter, as measured by DLS. (*E*) Zeta potential of the purified ivy nanoparticles dispersed in aqueous suspension, with a value of −29.0 ± 1.3 mV at 25 °C, as measured by ELS.

also retains the attachment feature of the English ivy toward substrates (Movie S1). Uniform and spheroidal organic nanoparticles were obtained after isolation and purification using size-exclusion HPLC (SEC-HPLC) (Fig. 1*B*) (23). As shown in Fig. 1*C*, the size of the purified individual ivy nanoparticles was ∼70 nm in diameter, as measured by AFM (18). Comparatively, in aqueous suspension, the hydrodynamic size of these nanoparticles was 109.6 ± 2.3 nm in diameter (Fig. 1*D*), with a negatively charged surface at pH 7.0 and a zeta potential of −29.0 ± 1.3 mV (Fig. 1*E*), as characterized by dynamic light scattering (DLS) and electrophoretic light scattering (ELS), respectively.

In light of the fact that the presence of glycoproteins in the ivy nanoparticles has been determined in recent biochemical assays (21, 23), we hypothesize that the ivy nanoparticles may consist of typical glycoproteins or proteoglycans present in the ECM of plant cells. Among them, one subfamily of hydroxyproline (Hyp)-rich glycoproteins (HRGPs), AGPs, seem to be the ideal candidates due to their vital roles in supporting the morphogenesis and function of root hairs (24–28). In the meantime, the AGPs have been detected in some other botanic adhesives (14–17). Additionally, the tertiary structure of the AGPs has theoretically been predicted to be spheroidal according to a wattle-blossom model, which was established to describe their 3D structure by analyzing the constituents and flexibility of the AGPs as a whole (24, 29–31).

To test whether AGPs are contained in the ivy nanoparticles, Yariv phenylglycoside dye, a reagent also called β-glucosyl Yariv (β-GlcY), which selectively binds to the AGPs via recognizing both given protein moieties and β-1,3-galactan chains with greater than five residues (24, 30, 32–35), was applied for identification. As shown in Fig. 2*A*, characteristic AGP-like smeared bands in a high molecular weight range were observed on respective SDS/PAGE gels stained with either Coomassie brilliant blue or 0.2% (wt/vol) β-GlcY dye (35, 36). Consistent with the gel information, the presence of AGPs in the purified ivy nanoparticles was further evidenced by Western blotting analysis using two mAbs, JIM13 and JIM14, which are commonly used to specifically recognize glycan epitopes of typical AGPs (see Table S1), as shown in Fig. 2*B*. In addition, FTIR spectroscopic measurements provided auxiliary evidence to support the existence of AGPs in the ivy nanoparticles, in comparing the IR spectra of the ivy nanoparticles with those of a standard reference AGP, gum arabic (Fig. S1). Furthermore, it was observed that the ivy nanoparticles exhibited photoelectron spectra similar to those of the gum arabic, as measured by X-ray photoelectron spectroscopy (XPS) (Fig. S2). All of the information described above demonstrates that, as expected, the AGPs indeed exist in the purified ivy nanoparticles.
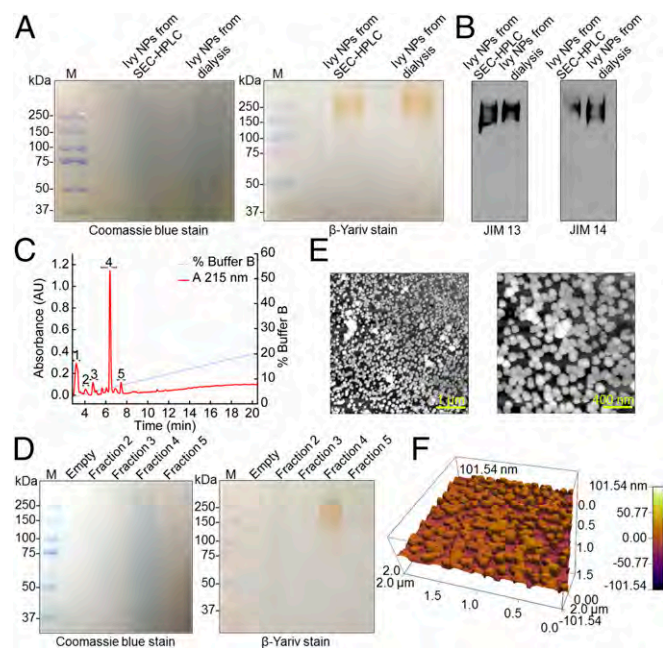


**Fig. 2.** Chemical identification of the purified ivy nanoparticles. (*A*) 10% (wt/vol) SDS/PAGE analysis of the ivy nanoparticles purified via two methods (either SEC or dialysis as described in *SI Materials and Methods*). Nanoparticles purified by SEC-HPLC or dialysis were loaded (30 μg per lane). The gels were stained with Coomassie brilliant blue (*Left*) and β-GlcY (*Right*), respectively. (*B*) Western blotting analysis of the purified ivy nanoparticles. Ivy nanoparticles purified by either SEC or dialysis were detected by anti-AGP (JIM13 and JIM14) mAbs. (*C*) RP-HPLC profile of the ivy nanoparticles harvested from SEC-HPLC. Via a gradient elution, five major fractions were collected and lyophilized. (*D*) Fractions 2–5, obtained from RP-HPLC, were examined by 10% (wt/vol) SDS/PAGE (30 μg per lane). Lane M, protein standard (marker); lane 1, empty; lanes 2 through 5, corresponding to respective fractions 2–5, obtained from RP-HPLC. The gels were stained with Coomassie blue (*Left*) and β-GlcY (*Right*), respectively. (*E*) AFM images of the fraction 4 obtained from RP-HPLC. Lyophilized fractions 2–5 were resuspended in water and applied to the coverslips for AFM scanning. Nanoparticles were only detected in fraction 4. [Scale bars, 1 μm (*Left*) and 400 nm (*Right*)]. (*F*) Three-dimensional AFM image of the fraction 4 obtained from RP-HPLC. The size is 2 μm × 2 μm, with a height bar on the right.

To further determine the proportion that AGPs account for in the purified ivy nanoparticles, RP-HPLC was carried out to segregate each noncovalently bonded structural domain. Upon gradient elution at a flow rate of 1 mL/min, a series of fractions were obtained, including one major and four minor ones, as shown in Fig. 2C. Apart from the solvent peak designated as fraction 1, all remnant fractions were loaded onto SDS/PAGE gels with equivalent amounts of samples (30 μg per lane). Among them, only the major fraction designated as fraction 4 was detected by Coomassie brilliant blue and β-GlcY simultaneously (Fig. 2D). Additionally, via weighing each lyophilized fraction, it was found that fraction 4 occupied up to 94% (wt/wt) of the entire amount, indicating that the vast majority of the components in the ivy nanoparticles consist of an AGP-rich fraction. Spheroidal nanoparticles, with an average diameter that resembled the purified ivy nanoparticles derived from SEC-HPLC, were observed in fraction 4 as examined by AFM (Fig. 2 E and F), whereas analogous nanoparticles were not detected in any other fractions, further suggesting that the minor fractions are nonessential constituents for the assembly of the overall architecture of the ivy nanoparticles. Given that structural domains with loosely noncovalent binding should have been separated during the gradient elution in RP-HPLC, these data suggest that the purified ivy nanoparticles observed in Fig. 1C are individual molecules, rather than clusters of multiple molecules. To our best knowledge, this architecture is by far the most regular spherical nanostructure obtained in AGP-rich molecules, and also in agreement with the wattle-blossom model (29).

**The Ivy Nanoparticles Are Rich in Acidic Arabinogalactan and Pectic Polysaccharides.** Given that the AGPs have been identified to be the predominant constituent in the ivy nanoparticles, an exploration of the detailed structures of the AGP molecules, including the monosaccharide composition, linkages, uronic acid content, and protein backbones, may allow us to elucidate the precise functions of the AGP-rich ivy nanoparticles involved in the generation of the strong adhesion strength. The glycosyl composition and linkages of sugar residues obtained from fraction 4 are listed in Table S2. Fraction 4 was rich in Gal and Ara, with respective proportions of up to 28.1% and 36.1% of the total monosaccharides, and 8.1% Rha, 9.6% GalA, 5.8% GlcA, 2.6% Xyl, 5.3% Glc, and 4.4% Man were also identified among the entire monosaccharides (Table S2). Moreover, the existence of type II arabinogalactans (AGs) in fraction 4 was validated by glycosyl linkage analysis, due to the presence of terminal Gal, as well as 3-, 6-, and 3,6-Gal residues (Table S2). In general, the ivy nanoparticles exhibit glycan structures homologous to typical AGPs in terms of the monosaccharide composition and linkages. Meanwhile, the detected GalA and pectic glycosyl linkages, including 2-, 2, 4-Rha, and 4-GalAp, also indicate the presence of rhamnogalacturonan-I (RG-I) and possible homogalacturonan (HG) in the ivy nanoparticles, as listed in Table S2. In combination with information gained from 1D $^1$H NMR spectra, which substantiated the existence of α-GalAp, α-Rhap, α-Araf, and β-Galp residues in fraction 4 (Fig. S3), evidence is sufficient to support the concept that the ivy nanoparticles are primarily composed of pectic AGPs, a bulky proteoglycan architecture similar to the arabinoxylan pectin arabinogalactan protein 1 and an RG-I–enriched fraction named Ara101P that are both identified in *Arabidopsis thaliana* (37). Notably, even though Glc, Man, and Xyl are not commonly regarded as characteristic monosaccharides in AGPs and pectin, they accounted for a proportion of greater than 12% (mole percent) of the total monosaccharides as a whole in fraction 4.

Typically, AGPs consist of core proteins and diverse *O*-glycans mainly comprising type II AGs and short oligoarabinosides (Fig. 3A) (24, 28, 30, 32, 38). It has been demonstrated that numerous AGP molecules possess negative surface charge that is thought
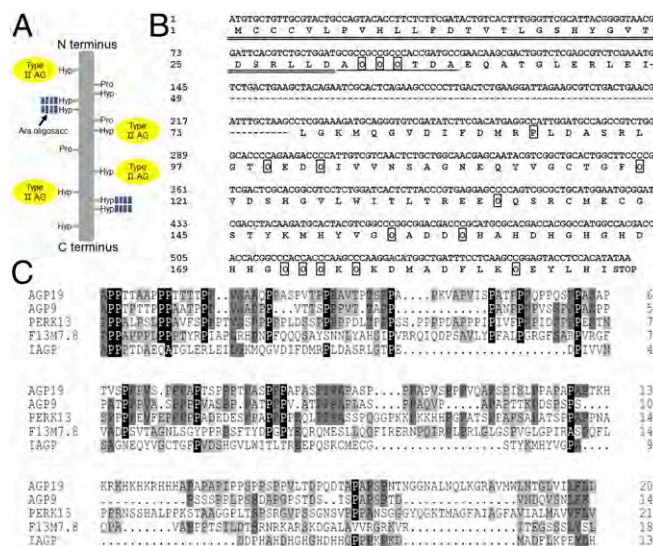


**Fig. 3.** Protein backbone of the AGP-rich ivy nanoparticles. (A) A schematic drawing of the glycosylated protein backbone. Proline residues are partially hydroxylated and glycosylated with either short oligoarabinosides or type II AGs (30, 38). (B) Amino acid sequence and corresponding nucleotide sequence of the protein backbone in the AGP-rich ivy nanoparticles. The amino acids obtained from N-terminal sequencing are single-underlined. O represents Hyp. The predicted signal sequence at the N-terminus is double-underlined. Genomic *iagp* contains an 83-bp intron that is indicated with a dashed line. Fifteen proline/Hyp residues (boxed) out of 132 aa were identified in the core protein. The number and the positions of the Hyps were determined by subsequent MALDI-TOF MS. (C) Multiple sequence alignment of IAGP with four other HRGPs in *Arabidopsis*. These four glycoproteins were chosen for multiple sequence alignment because they are the most analogous HRGPs to the IAGP, according to a BLASTp search in *A. thaliana*. The alignment was generated by ClustalX and edited manually using DNAman. Identical residues are shaded in black, and conserved and similar residues are indicated in dark gray and light gray, respectively.

to be associated with the presence of uronic acid substituents (i.e., GlcA and GalA) at the termini of type II AGs (24, 29, 30). In this respect, likewise, the negative surface charge exhibited by the ivy nanoparticles (Fig. 1E) presumably arises from the deprotonation of GlcAp and GalAp residues in solution.

**Core Protein Constitutes the Framework for the Construction of the AGP-Rich Nanoparticle.** In addition to the monosaccharide composition and linkages, the core protein that constitutes the framework for the construction of the overall architecture of the ivy nanoparticle was also explored. For such a purpose, the AGP-rich fraction gathered from RP-HPLC (i.e., fraction 4) was deglycosylated and a short segment of an amino acid sequence at the N terminus of the deglycosylated protein, Ala-Hyp-Hyp-Hyp-Thr-Asp-Ala, was determined via Edman degradation. According to this N-terminal sequence, degenerate primers were designed and the nucleotide sequence for the full-length cDNA encoding the core protein was then determined by 5′- and 3′- RACE cloning (Fig. 3B). Moreover, the identified full protein sequence, designated as IVY ARABINOGALACTAN PROTEIN (IAGP), demonstrated a moderate similarity to four other HRGPs derived from *Arabidopsis* in a sequence alignment (Fig. 3C). Notably, in a BLASTp search in the genome of the *A. thaliana*, the IAGP identified from *H. helix* also exhibited a moderate extent of similarity to several cytochrome *c* oxidase subunits, implying potential homology between these two types of proteins. Accordingly, a phylogenetic analysis was carried out to determine the relationship of the IAGP with these analogous proteins obtained from BLASTp. Among them, the IAGP and the AGP9 were the closest relatives, as shown in Fig. S4A. The identity

of the IAGP obtained from the RACE cloning was further validated by MALDI-TOF MS analysis by determining the masses of the tryptic peptides of the deglycosylated fraction 4 obtained from RP-HPLC. As shown in Fig. S4B, three peptides with respective masses detected by the MS matched the predicted molecular masses of expected tryptic peptides. Additionally, the degree of hydroxylation and the distribution of the Hyps in other estimated tryptic peptides were deduced from relevant molecular masses gained from the MS test. Given that greater than 90% of the prolines within the IAGP appear in the form of Hyp, which commonly bears type II AGs and short oligoarabinosides in typical AGPs (29, 30), the IAGP should be highly O-glycosylated in the ivy nanoparticles, similar to other AGPs identified from A. thaliana.

**Spherical AGP-Rich Nanoparticles Favor Surface Wetting.** To explore the potential molecular mechanisms that allow the AGP-rich nanoparticles derived from English ivy to intensify the surface adhesion, the intrinsic viscosity of the purified ivy nanoparticles was examined. As expected, similar to a variety of typical AGPs, AGP-rich ivy nanoparticles exhibited an exceedingly low intrinsic viscosity in solution ($[\eta]_{ivy\ NPs} = 30.4 \pm 1.9$ mL/g), whereas ~3.7-fold

higher intrinsic viscosity was obtained in gum arabic, and ~8- to 20-fold higher viscosities were observed in pectin and sodium alginate, respectively, as shown in Fig. 4A. Given that the low intrinsic viscosity is commonly regarded as the most exceptional physical trait with respect to the AGPs (24, 29, 30), and the wattle-blossom theoretical model proposed previously has associated this low intrinsic viscosity with the anticipated spheroidal appearance of the majority of the AGPs (24, 29, 30), it is logical to expect the potential correlations between this physical property and the physiological activities of the AGP-rich ivy nanoparticles within the adhesive exudates, even though the implication of this physical property during the growth and development of plants has not been illustrated in the earlier studies (24, 29, 30). Accordingly, a pivotal aim of this study is to elucidate the physiological meanings relevant to the low intrinsic viscosity of the AGP-rich ivy nanoparticles in H. helix.

In most cases, to realize ideal adhesive action, an engineered synthetic glue may be designed and optimized to ensure preferable functionalities in two aspects: a favorable wetting behavior on the surface and an effective strategy to originate sufficient adhesion strength during the subsequent curing (hardening) procedure
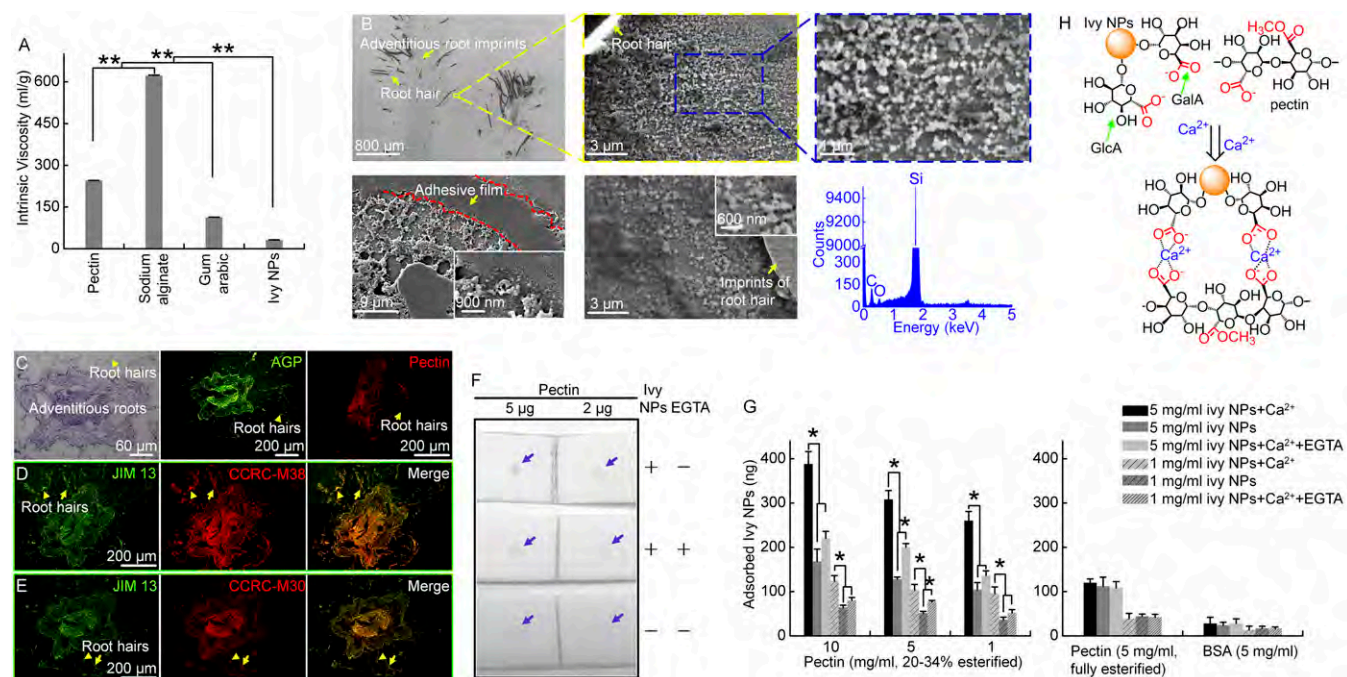


**Fig. 4.** Unlocking the molecular mechanisms underlying the ivy-derived adhesive. (A) Intrinsic viscosities of the ivy nanoparticles, gum arabic, pectin, and sodium alginate, as measured by capillary viscometer. Ivy nanoparticles ($[\eta]_{ivy\ NPs} = 30.4 \pm 1.9$ mL/g) and gum arabic ($[\eta]_{gum\ arabic} = 112.5 \pm 1.2$ mL/g) exhibited markedly lower intrinsic viscosities, in contrast to the pectin ($[\eta]_{pectin} = 244.8 \pm 0.7$ mL/g) and the sodium alginate ($[\eta]_{sodium\ alginate} = 622 \pm 2.1$ mL/g) ($P < 0.01$). Error bars indicate SD; **$P < 0.01$, using one-way ANOVA and Tukey's post hoc test. (B) (Upper Left) SEM image of the imprint of the adventitious roots on a silicon wafer. (Scale bar, 800 μm.) (Upper Middle) Enlarged SEM image. Nanoparticles exhibited a strong tendency to cluster and form bulky pads. (Scale bar, 3 μm.) (Upper Right) Further-enlarged SEM image. (Scale bar, 1 μm.) (Lower Left) SEM image of the film formed by the ivy adhesive. (Inset) A high-magnification view of the film. (Scale bars, 9 μm and 900 nm, respectively.) (Lower Middle) SEM image of the dried exudates. Nanoparticles were observed to be embedded in a gel-like porous network. (Inset) High-magnification view. (Scale bars, 3 μm and 600 nm, respectively.) (Lower Right) EDX spectra of the exudates remnant on the silicon wafer. Apart from silicon, the vast majority of the surface elements were carbon and oxygen. (C) Immunofluorescent localization of the AGPs and the pectic polysaccharides in root sections of H. helix. (Left) A cross-section of the adventitious root stained by toluidine blue. (Scale bar, 60 μm.) (Middle) A cross-section of the adventitious root immunostained by anti-AGP mAb JIM13. (Scale bar, 200 μm.) (Right) A cross-section of the adventitious root immunostained by anti-pectin mAb CCRC-M38. (Scale bar, 200 μm.) (D) (Left) A cross-section of the adventitious root coimmunostained by mAbs JIM13 and CCRC-M38. FITC signal (AGPs) was captured. (Middle) The same coimmunostained section. R-Phycoerythrin signal (pectin) was captured. (Right) A merged image. (Scale bar for all panels, 200 μm.) (E) A cross-section of the adventitious root coimmunostained by mAbs JIM13 and CCRC-M30. FITC signal (AGPs) and R-Phycoerythrin signal (pectin) were captured, respectively. (Scale bar for all panels, 200 μm.) (F) Dot blotting test. Stronger dot signal suggests higher level of the AGP-rich ivy nanoparticles arrested by the adsorbed pectin on the PVDF membrane. (G) Fluorescent combination assay. The amount of the FITC-conjugated ivy nanoparticles bound by the 20–34% esterified pectic polysaccharides was calculated according to a calibration curve for fluorescent intensity vs. concentration. Error bars indicate SD; *$P < 0.05$, using one-way ANOVA and Tukey's post hoc test. Calcium-dependent binding between the AGP-rich ivy nanoparticles and the BSA/the fully methyl-esterified pectin was not noticeable. (H) A schematic drawing of the $Ca^{2+}$-driven cross-linking among carboxyl groups of uronic acid residues within the AGPs and the pectic acids.

(26, 39–44). Analogous to a series of conventional glues, to accomplish adhesion at the interface, the sticky exudates derived from English ivy should initially wet the surface, a spreading motion capable of driving an intimate and extensive contact over the substrates. In light of the established wetting theory, the liquid adhesives with lower viscosities typically exhibit a better wetting performance than the highly viscous glues (39, 40, 45–47). Thereby, in the case of the ivy adhesive, the comparatively low intrinsic viscosity of the AGP-rich ivy nanoparticles in solution is beneficial for the wetting activity that can be achieved by the ivy adhesive. Additionally, owing to their tiny scale, these nanosized spheroidal particles are also exceptional in penetrating surface irregularities present on most substrates, further promoting intimate interactions between the ivy-derived adhesive and corresponding substrates.

**Aggregation of Spherical Nanoparticles Toward the Formation of Adhesive Film.** Apart from the wetting activity favored by the low intrinsic viscosity of the AGP-rich ivy nanoparticles, as a typical structural adhesive, in principle, a curing step is required for the ivy-derived adhesive to create sufficient cohesive strength within the exudate, aiding in the formation of strong adhesion strength at the interface (26, 39–44). Commonly, curing (hardening) of adhesives arises from water evaporation and/or chemical cross-linking (26, 39–44). Notably, in the earlier studies, morphological descriptions with respect to the drying process involved in the curing of botanic adhesives derived from the adventitious roots of English ivy (18), and the climbing organs of analogous plants (15), have substantially advanced our understanding of the relevant molecular events regulating the adhesive action in the plant kingdom.

To investigate the hardening of the ivy-derived adhesive in detail, and the role of the AGP-rich ivy nanoparticles in promoting this process, a cultivation platform was developed to collect and observe the sticky exudate in situ, as shown in Fig. S5. Throughout the secretory and curing progress, traces left on the surface of the fixed silicon wafers were monitored using SEM. It was observed that considerable spheroidal nanoparticles were secreted on the silicon wafers, present around the imprints of the adventitious roots of English ivy, demonstrating an average size similar to those extracted and purified in vitro, as shown in Fig. 4B, Upper. In addition, the ivy nanoparticles remnant on the silicon wafers exhibited a strong tendency to cluster, forming bulky pads at the interface (Fig. 4B, Upper Middle and Upper Right). Given that the AGPs are characterized by their capacity to agglomerate, as described in the previous study (24), it is reasonable to propose that the aggregation of the ivy nanoparticles within the sticky exudate is driven by the physicochemical interactions of the AGPs. Consistently, in the case of the AGP-rich nanoparticles isolated and purified in vitro by means of SEC-HPLC, a similar agglomerate fashion of nanoparticles over time was also observed, as shown in Fig. S6. Furthermore, the agglomerate progress of the nanoparticles toward bulky pads demonstrated a trend in the formation of a compact film at the interface, implying the pivotal roles of the spheroidal nanoparticles within the exudates during the curing procedures (Fig. 4B, Lower Left and Fig. S7). Meanwhile, energy-dispersive X-ray (EDX) spectra showed that apart from a silicon signal derived from the substrate, the vast majority of the surface elements were carbon and oxygen, suggesting the organic nature of these nanostructures (Fig. 4B, Lower Right).

**Calcium-Dependent Cross-Linking Drives the Curing of the Ivy-Derived Adhesive.** In addition to the abundant spherical nanoparticles observed in the periphery of the imprints of the root hairs, a translucent gel-like porous network comprising tightly cross-linked spheres in nanoscale was also captured in the adhesive remnant on the silicon wafers by SEM observation (Fig.

4B, Lower Middle). To determine the chemical constituents of this matrix, the remnant substances exuded from the adventitious roots on the silicon wafers were resuspended in PBS and examined using the ELISA screening test, with 38 mAbs raised against the vast majority of the polysaccharides present in the plant cell wall listed in Table S1. As shown in Fig. S8, accompanied by AGs, diverse pectic epitopes are also richly distributed in the adhesive secretions. Moreover, a subsequent glycosyl composition assay identified that 4.09% (mole percent) of GalA$p$ residues were contained in the adhesive substances recovered from the remnant on the silicon wafers, as listed in Table S3, further suggesting the existence of pectic polysaccharides in the mucilage derived from the adventitious roots of English ivy. Meanwhile, from the monosaccharide composition analyses, it is also noteworthy that the proportion of Glc, Man, and Xyl as a whole is greater than 65% (mole percent) of the total monosaccharides, suggesting the presence of cellulose and/or hemicellulose in the imprints remaining on the silicon wafers. These substances presumably arise from the encapsulation of partial components of the plant cell wall within the cured adhesive, a phenomenon that has been detailed in the previous studies (15, 18). Given that AGs and pectic substances have been identified to be two of the predominant components in the majority of botanic adhesives, including those obtained from the climbing organs of Virginia creeper, Boston ivy, and *Ficus pumila*, as shown in the previous cytochemical analyses (14–17, 48–50), it is logical to expect that these two acidic polysaccharides possess exceptional capacity to effectively support the adhesive function of the sticky exudates at the interface. In particular, for the mucilage secreted by the root hairs of English ivy, the pectic acids may exist alone and/or be covalently bonded to the AGPs within the ivy nanoparticles as interpreted above. More evidence regarding the coexistence of the AGPs and the pectic polysaccharides within the extracellular matrix of ivy root cells was obtained from the subsequent immunohistochemical assessment, as shown in Fig. 4 C–E, further implying the functional correlations between these two components. In this respect, the effort in the exploration of the potential interactions among these acidic polysaccharides/glycoproteins may substantially improve our understanding of the molecular events controlling the generation of strong adhesion strength within the ivy-derived bioadhesive. For such a purpose, a dot blotting test and a fluorescent combination assay were carried out to evaluate the hypothetical binding between the AGP-rich ivy nanoparticles and the pectic polysaccharides, apart from the aforementioned covalent conjugation of the AGPs and the short fragments of pectin within the ivy nanoparticles. As shown in Fig. 4F, although the AGP-rich ivy nanoparticles indeed demonstrated concentration-dependent interactions with the adsorbed pectic polysaccharides in the dot blotting test, this binding was susceptible to the addition of external $Ca^{2+}$-chelating agent, EGTA, which apparently suppressed the binding affinity of these two components. Additionally, this electrostatic interaction was further quantitatively evaluated using a fluorescent combination assay. As expected, the concentration-dependent interactions between the ivy nanoparticles and the pectic polysaccharides were consistently observed in this assay, as shown in Fig. 4G. In the meantime, for the ivy nanoparticles tested at an initial concentration of 5 mg/mL, the amounts of the immobilized ivy nanoparticles detected in the incubation buffers containing 2 mM $Ca^{2+}$ were ~2.1- to 2.5-fold and 1.5- to 1.8-fold greater than those of the nanoparticles remaining in $Ca^{2+}$-free buffers and EGTA-containing buffers, respectively, at pectin concentrations ranging from 1 to 10 mg/mL. This suggests that the calcium ions are capable of promoting the electrostatic binding of the AGP-rich ivy nanoparticles and the pectin. To further validate this $Ca^{2+}$-dependent interaction, 1 mg/mL ivy nanoparticles were applied to the combination assay under the same condition. As

shown in Fig. 4*G*, in comparison with respective amounts of the ivy nanoparticles attached to the adsorbed pectic polysaccharides either in the absence of calcium ions or in the presence of excess EGTA, at least 2.0- and 1.2-fold greater amounts of the FITC-conjugated nanoparticles were detected to be bound to the pectin in the EGTA-free reaction buffer containing 2 mM $Ca^{2+}$. In addition, this $Ca^{2+}$-modulated electrostatic interaction between the AGP-rich ivy nanoparticles and the pectic polysaccharides upon binding was further evidenced by testing the binding affinity of the AGP-rich ivy nanoparticles toward other electroneutral molecules, including BSA and fully esterified pectin, in the same assay. As shown in Fig. 4*G*, in contrast to the case containing 2 mM $Ca^{2+}$, a significant difference in the amount of the FITC-conjugated nanoparticles attached after 1-h incubation was not observed in response to either the absence of calcium ions or the presence of external EGTA, indicating that the calcium ion-driven interaction between the AGP-rich ivy nanoparticles and the acidic pectic polysaccharides is the predominant force aiding in their binding. This electrostatic interaction is displayed by calcium ions in facilitating the cross-linking among carboxyl groups of the uronic acid residues within the AGPs and the pectic acids (Fig. 4*H*). It is noteworthy that this $Ca^{2+}$-driven event has been frequently discussed in the earlier reports (24, 31, 51), with experimental results consistent with that of the current study. Meanwhile, given that $Ca^{2+}$ is one of the richest and most physiologically vital ions present in the extracellular space of plant cells (52–54), it is reasonable to conclude here that the $Ca^{2+}$-regulated cross-linking among these acidic polysaccharides/glycoproteins undoubtedly renders a potent driving force, effectively promoting the curing (hardening) progress of the sticky exudate derived from the adventitious roots of English ivy. In particular, under natural conditions, AGPs have shown a trend in raising the porosity of the native pectic gel, functioning as "pectin plasticizers" as described previously (28, 30, 55). In this respect, it is reasonable to propose here that in the ivy-derived adhesive, uronic acid-rich AGPs and pectic polysaccharides cross-link to form a porous network upon hardening, an architecture shown in the SEM observation as mentioned above (Fig. 4*B*, *Lower Middle*).

**High-Strength Adhesion Is Achieved by the Interactions of the AGPs and the Pectin Within the Ivy Adhesive.** In light of the information gained from the overall study, the molecular basis for the ivy-derived adhesive at the interface is envisaged and summarized as follows (Fig. 5). Initially, for the attachment, the AGP-rich ivy nanoparticles are secreted toward the extracellular space of root cells upon contact with corresponding substrates in a manner that has been monitored in real time in our recent study (19). These spheroidal nanoparticles are concentrated during evaporation, and the highly structural flexibility of the protein backbone as well as the anchored bulky AG branches of the AGPs allow these macromolecules to be tightly packed (29), reaching an intimate connection between adjacent nanoparticles. Subsequent $Ca^{2+}$-driven cross-linking among carboxyl groups of the uronic acid residues within the AGPs and the pectic acids in the extracellular space favors the cohesion of the adjacent AGP-rich nanoparticles, gives rise to the generation of an adhesive film (24, 31, 38), further aids in the curing progress of the exuded adhesive, and eventually realizes the adhesive function at the interface by restraining the relative movement of the adventitious roots and the corresponding substrates. Throughout these procedures, the AGP-rich ivy nanoparticles also possess the capacity to permeate irregularities present on the substrates owing to their rough surfaces in most cases, resulting in a strong mechanical interlocking at the interface and further ensuring an ideal adhesive action (26, 39, 40, 42–46). In addition to the calcium-dependent electrostatic interactions and mechanical interlocking, the van der Waals force is also evidenced to be
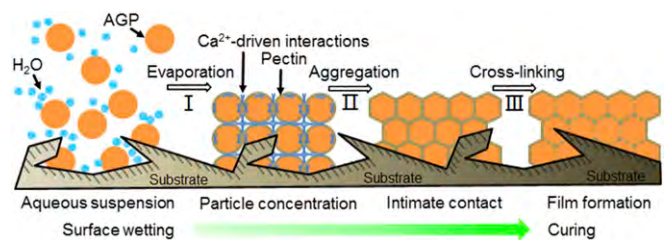


**Fig. 5.** A schematic drawing of the molecular basis for the ivy-derived adhesive. Adhesive substances are exuded toward the extracellular spaces of root cells, containing AGP-rich nanoparticles, in a manner that has been documented earlier (19). The spheroidal shape of these nanoparticles allows them to be liable to spread at the interface and permeate the substrates, as a result of their low intrinsic viscosity. Upon evaporation, nanoparticles are concentrated and packed to reach tight contact, giving rise to the formation of a film. Further calcium-dependent cross-linking among carboxyl groups of the AGPs and the pectic polysaccharides elevates the cohesive strength of this film, and the intimate contact of the nanoparticles with the corresponding substrates causes an effective mechanical interlocking at the interface.

involved in the curing process, as interpreted in our previous study (56).

**Reconstruction of an Ivy-Mimetic Adhesive Composite to Validate the Adhesion Mechanisms.** In light of the uncovered molecular basis for the ivy-derived adhesive, a reconstructed biomimetic adhesive was subsequently developed by integrating the purified ivy nanoparticles with pectin in the presence of 2 mM calcium ions, to offer an engineering instance that might further evidence the putative adhesion mechanisms summarized above. To evaluate the behavior of the prepared adhesive composites, the adhesion strength of this reconstructed adhesive was examined by both the lap joint shear strength test and the tensile strength test, two strategies that have been extensively applied to quantitatively assess bioadhesives (Fig. 6*A*) (42, 43, 57–59). The variation in shear strength of the prepared adhesive constructs was monitored over time to reflect the curing progress. As shown in Fig. 6*B*, the shear strength of the ivy-mimetic composites at failure was elevated with increasing time and reached a plateau of maximum value in approximately 3 d. To explore the specific roles of each component within the developed material, the shear strengths of the $Ca^{2+}$-free and EGTA-containing adhesive constructs, as well as those of the individual ivy nanoparticles/pectin incorporated with calcium ions, were also traced throughout the test under the same conditions. Similarly, the maximal shear strengths of the respective control groups could not be approached for approximately 3 d. However, a significant difference in the shear strength values that could be reached after 3 d was observed among distinct adhesive composites. On day 7, a shear strength up to $0.53 \pm 0.033$ MPa was achieved by the ivy-mimetic adhesive construct prepared in the presence of $Ca^{2+}$ and in the absence of EGTA, substantially greater than those of the $Ca^{2+}$-free or EGTA-containing counterparts, with respective shear strengths of $\sim 0.31 \pm 0.013$ and $0.40 \pm 0.010$ MPa, indicating the significance of the calcium ions in developing an ivy-mimetic adhesive composite with the expected level of performance. Meanwhile, the shear strengths of the composites consisting of 2 mM $Ca^{2+}$ integrated with either ivy nanoparticles or pectin alone were $\sim 0.12 \pm 0.036$ and $0.40 \pm 0.017$ MPa, respectively, still markedly weaker than that of the ivy-mimetic adhesive constructs 7 d after preparation. The stress-strain curves of respective adhesive composites, as measured and plotted by the lap shear test on day 7, are shown in Fig. 6*C*. It could be observed that, for the adhesive composites comprising both the ivy nanoparticles and pectic polysaccharides, the strains at failure were substantially lower than those of the constructs containing either ivy nanoparticles or pectic substances alone. In particular, the minimum strain at failure was
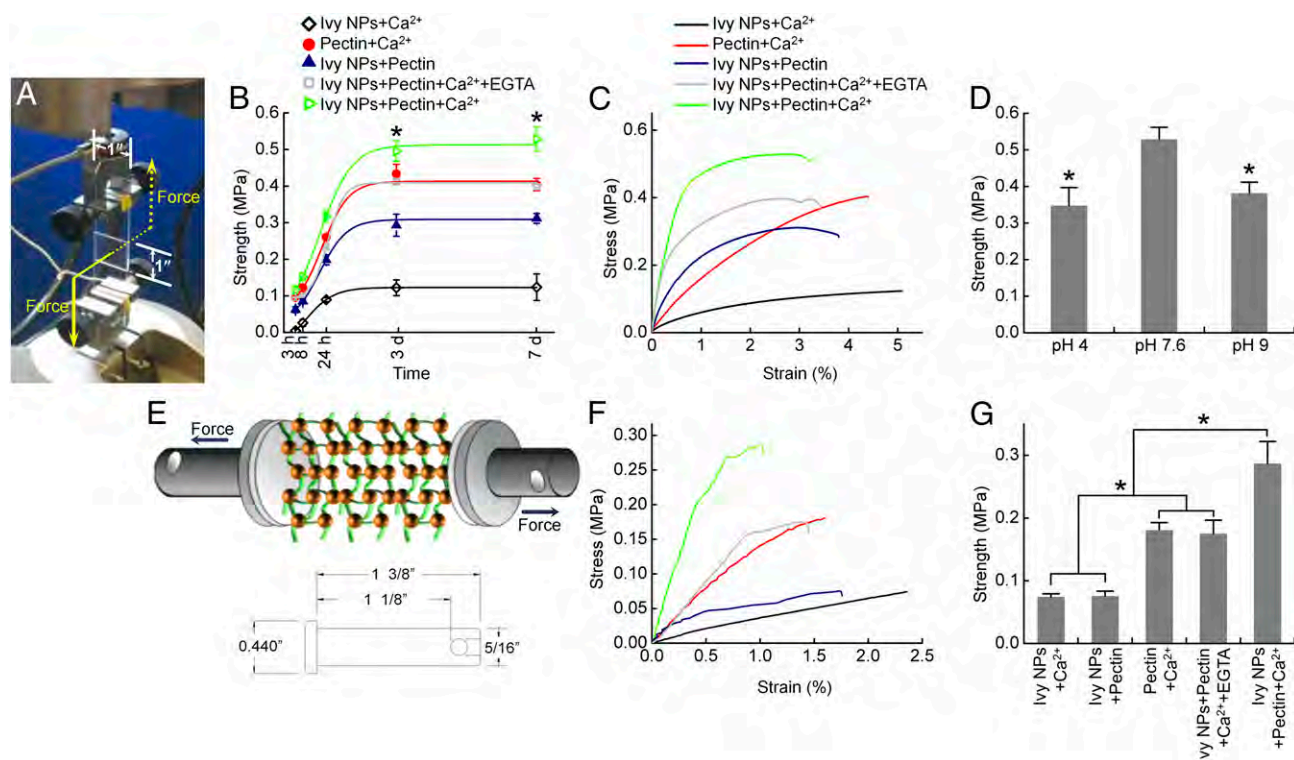
**Fig. 6.** Tensile test of the reconstructed ivy-mimetic adhesive composites. (*A*) For the adhesive lap joint shear strength test, prepared adhesive composites were applied to a 1-inch × 1-inch overlapping area of two glass slides. (*B*) Shear strengths of the ivy-mimetic adhesive composites 3 h, 8 h, 24 h, 3 d, and 7 d after preparation. The shear strengths of the calcium-free and EGTA-containing adhesive constructs, as well as the composites consisting of individual pectin/ivy nanoparticles and $Ca^{2+}$, were also measured at the same time intervals, respectively. The strength curves were fitted by OriginPro 8.0 using a growth/sigmoidal function ($y = \frac{A2-A1}{1+10^{(LOGx0-x)\,p}} + A1$). Error bars indicate SD; *$P < 0.05$, in comparing the shear strengths of the EGTA-free adhesive composites in the presence of 2 mM $Ca^{2+}$ to those of all other groups, using one-way ANOVA and Tukey's post hoc test. (*C*) Stress-strain curves of respective composites measured by lap shear test 7 d after preparation. (*D*) Influence of pH value on the shear strengths of the ivy-mimetic adhesive constructs, as measured by lap shear test on day 7. Error bars represent SD; *$P < 0.05$, vs. the shear strength of the composites prepared at pH 7.6. (*E*) (*Upper*) A schematic drawing of the adhesive tensile strength test. Adhesive composites were applied to the interface of two clevis pins and the tensile strength was examined on an MTS system as shown in A. (*Lower*) The dimensions of the clevis pin used in this test. (*F*) Stress-strain curves of respective composites measured by adhesive tensile strength test 7 d after preparation. (*G*) Tensile strengths of respective adhesive composites on day 7. Error bars indicate SD; *$P < 0.05$, using one-way ANOVA and Tukey's post hoc test.

reached by the ivy-mimetic EGTA-free adhesive composite in the presence of $Ca^{2+}$.

In addition to the apparent effects of the ionic strength, the influence of pH value on the shear strength of the reconstructed ivy-mimetic adhesive was also evaluated by preparing the adhesive composites at distinct pH. As shown in Fig. 6*D*, in comparison with that of the adhesive composite prepared under neutral condition, slightly but significantly weaker shear strengths obtained on day 7 were observed in response to the pH variations. In particular, in contrast to the composite prepared in Tris-buffered saline (TBS) at pH 7.6, ~1.4- to 1.5-fold lower shear strengths were reached by the cases prepared at pH 4 or 9 after 7 d. Given that the cross-linking extent of the ivy-mimetic adhesive constructs is determined by the calcium-modulated electrostatic interaction that is susceptible to pH variations, it is reasonable to expect this pH-responsive event here. Because the $pK_a$ of pectin is ~3.5 (60, 61), and the isoelectric point of the AGP-rich ivy nanoparticles should be located in the acidic range given their negative charge displayed under neutral condition (Fig. 1*E*), the deprotonation of the carboxyl groups of the uronic acid residues within both components is suppressed at pH 4 in contrast to that in a neutral environment, resulting in less surface charge and thus weaker electrostatic interactions with calcium ions. On the contrary, $Ca^{2+}$ is prone to form slightly soluble $Ca(OH)_2$ under an alkaline condition (pH 9), also undermining the electrostatic binding. In both cases, the cross-linking degree of the adhesive composites is affected upon the curing process, giving rise

to lower adhesion strengths than that of the adhesive material prepared at pH 7.6.

To ideally reflect the interfacial behavior of the reconstructed ivy-mimetic adhesive composites, an alternative tensile strength test was performed by applying the prepared adhesive materials to the joint of two clevis pins, as illustrated in Fig. 6*E*. Similar to the information gained from the lap shear test, the stress-strain curves show that the strain at failure of the reconstructed ivy-mimetic adhesive composite in the presence of $Ca^{2+}$ and in the absence of EGTA is ~57% and 37% lower than those of the cases containing 2 mM $Ca^{2+}$ integrated with either ivy nanoparticles or pectic polysaccharides, respectively, on day 7 (Fig. 6*F*). In addition, the tensile strength of this reconstructed ivy-mimetic adhesive composite was ~3.9-, 1.6-, 3.8-, and 1.7-fold stronger than respective adhesive composites consisting of ivy nanoparticles with $Ca^{2+}$, pectin with $Ca^{2+}$, ivy nanoparticles with pectin, or ivy nanoparticles with pectin in the presence of both $Ca^{2+}$ and EGTA, 7 d after preparation, as shown in Fig. 6*G*.

## Discussion

**The Uniqueness of the Ivy Adhesive in Contrast to Other Botanic Adhesives.** One of the early efforts in exploring the behaviors of bioadhesives derived from climbing plants was made by Charles Darwin, who described and documented the process of the "viscid fluid" exuded by the adventitious roots of *Ficus repens* (62). Since then, unfortunately, few studies have dealt with the

molecular events within the botanic adhesives, and, accordingly, little is known about the adhesion mechanisms underlying these mucilages. In recent years, the chemical components of several types of botanic adhesives produced by Virginia creeper (*Parthenocissus quinquefolia*), Boston ivy, and *F. pumila* have been examined by immunocytochemical identification and cytochemical stains (12, 14–17). Consistently, acidic polysaccharides and glycoproteins, involving pectic acids, AGs, and AGPs, are recognized as the predominant constituents of these adhesive substances. As a result, production of a pectic mucilage that sets and adheres the vines to the support surfaces is thought be involved in the clinging of most climbing plants (14). Additionally, AGs and AGPs are hypothesized to be the highly mobile phase within the botanic adhesives, capable of penetrating the interstices of the substrates and facilitating the sealing of the adhesives into numerous tiny holes on the surface of the support substrates (14, 63). Vaughn and Bowling (63) have appropriately described the pectins and the AGPs in the botanic adhesive as "mucilaginous molecules that are spread across the surface of the structure to be attached, filling in the gaps." In particular, "arabinans and AGPs appear to be an even more mobile component of the adhesive, filling in spaces between the papillate epidermal cells and even moving into small cracks in the structure that is attached" (63). In this study, pectic polysaccharides and AGPs are also identified to be the predominant components of the mucilage exuded by the adventitious roots of English ivy and the AGPs are substantiated to be present in a nanosized spherical appearance within the sticky liquid. These spherical architectures are the most unique feature that distinguishes the ivy adhesive from other botanic mucilages. The spherical shape results in the low intrinsic viscosity of the AGP molecules and thus allows a favorable surface wetting of bioadhesive over the support surfaces. In this respect, this study provides the first experimental evidence to our knowledge to support the hypothetical theory that the AGPs serve as a mobile phase in the adhesive exudates. More importantly, the molecular interactions within the ivy-derived adhesive were investigated in detail and calcium-dependent electrostatic binding between uronic acid residues on the pectic substances and the AGPs is evidenced to be the driving force for the effective cross-linking (curing) of the mucilage. Analogous or identical molecular events might be present in other botanic adhesives owing to their similar functions and chemical constituents.

**New Insight into the Physiological Functions of AGPs and Pectin.** As one of the most intricate glycoprotein families present in the extracellular space of plant cells (24, 30, 64, 65), the diversity of the protein backbones and the complexity of the anchored *O*-glycans allow the AGPs to be involved in numerous aspects of growth and development. In particular, it has been demonstrated that the AGPs are capable of aiding in the formation of pollen tubes, facilitating cellular communication, inducing and adjusting the release of regulatory factors, and participating in many other cellular events (24). In addition to those identified in the adhesive substances exuded by climbing plants, the AGP molecules are also thought to exert adhesive function on the stigma surface, acting as an adherent base for capturing pollen, as evidenced in the earlier studies (65–68). Here, we hypothesize that the AGP-rich nanoparticles exuded by the adventitious roots of English ivy may be involved in molecular events similar to those observed on the stigma surface. In this respect, the efforts in the identification of the roles of the AGP-rich ivy nanoparticles in the generation of strong adhesion strength may considerably improve our understanding of a series of adhesion behaviors throughout the plant kingdom. In contrast, pectin has been thought of as an adhesion molecule for a long time due to its capacity to be internally cross-linked, supported by calcium salt bridges (69). Owing to its adhesive property, pectin has been exploited in numerous commercial glues (70, 71). In addition,

pectin is involved in a cascade of adhesion events during the formation of the plant cell wall and is necessary for the adhesion of pollen tubes (69, 72). Here we show that the pectic polysaccharides exhibit a similar adhesion function in the ivy-derived mucilage via the electrostatic interactions with AGP molecules. The molecular bases for this botanic adhesive might provide some hints for elucidating other adhesive events in which the pectin is involved.

**New Evidence to Support the Wattle-Blossom Model.** In this study, the spherical nanoparticles observed in the mucilage exuded by the adventitious roots of English ivy are identified to be predominantly composed of AGPs, a superfamily of HRGPs present in the plant cell wall. These AGP-rich nanoparticles were harvested by a physical strategy based on size-exclusion chromatography, rather than other chemical approaches that have been extensively used for the preparation of conventional AGP molecules, including Yariv precipitation and immunoaffinity recognition (24, 30). The inherent morphological traits of the AGPs in the natural environment, as a result, might be maximally preserved by means of this physical isolation procedure. Meanwhile, in the previous studies, despite AGPs having been theoretically predicted to possess a spheroidal appearance owing to their low intrinsic viscosities in solution, according to the wattle-blossom model (24, 29, 30), the informative value of the viscosity with regard to the plant physiology is still elusive (29, 30). In this respect, our current study not only serves as evidence to support the theoretical prediction regarding the tertiary structures of the AGPs but also elucidates the physiological meaning of the low intrinsic viscosity.

**Similarities Between the Ivy Adhesive and the Animal Adhesives.** Notably, it has been proposed that the genes encoding the HRGPs may originate from a "superfamily" of ancient genes relevant to diverse adhesive events in both animals and plants (26). In comparing the cell walls of plants to the corresponding extracellular matrices of animals, with respective frameworks built with HRGP extensin family and collagen, obviously, considerable commonalities are shared by these two types of polymeric networks (26). In particular, repeat motifs dominated by Hyp are observed in both matrices, defining and determining the helical conformation during the complicated assembly and cross-linking process (73). Meanwhile, the helical conformation is thought to be stabilized by the arabinosyl/galactosyl modification of the Hyps within both networks (26, 73). Interestingly, a similar Hyp-rich motif is also identified in the adhesive proteins isolated from mussel (4, 74), suggesting potential evolutionary homology between the adhesive proteins derived from animals and plants (26). As another typical subfamily of HRGPs, the AGPs identified in the ivy nanoparticles are also rich in Hyp. In this respect, there may be still some ubiquitous principles between these two types of bioadhesives waiting for us to explore.

**Bioinspired Engineering Application of the Adhesion Mechanisms Revealed by English Ivy.** The manner in which nanosized particles are involved during the formation of an adhesive film between two adherends has been well elucidated in the case of the poly(vinyl acetate) adhesive, which is a conventional glue prepared by means of emulsion polymerization (40, 75–79). Typically, commercially available poly(vinyl acetate) glues are comprised of synthetic particles in nanoscale dispersed in aqueous suspension (76–79). After being applied to a substrate, a three-step strategy was used by this glue to accomplish adhesive activity at the interface, including (*i*) tight packing of the particles upon evaporation, (*ii*) deformation of the particles toward intimate interactions, and (*iii*) coalescence (cross-linking) between adjacent particles to create a cohesively strong solid (76–79). Analogously, these engineered synthetic nanoparticles boost the mechanical interlocking of the glue at the interface in a pattern similar to that of the spheroidal nanoparticles

observed in the ivy-derived adhesive, as documented in the previous reports (39, 40, 75, 80, 81). In this respect, in contrast to the consecutive molecular events in which the AGP-rich ivy nanoparticles are involved as detailed above, it is logical to propose here that these two types of polymeric nanoparticles share considerable mutual principles underlying their respective adhesive activities. Furthermore, in terms of the engineering applications, given that one typical AGP-rich molecule, gum arabic, has been extensively developed as commercial glues in the stamp industry (24), the insights into the principles controlling the molecular interactions within the ivy-derived adhesive substances, provided by this study, may have broader impacts on offering guidelines for directing the design and fabrication of engineered or biomimetic glues. In the current study, we reconstructed an ivy-mimetic adhesive composite in light of the molecular bases proposed, and the subsequent tensile tests suggest that it not only in turn validates the adhesion mechanisms underlying the ivy-derived mucilage but also offers a template for exploring the feasibilities of developing ivy-inspired engineered glues with desirable functionalities in the future.

**Conclusions and Future Prospects.** To summarize, the AGP-rich ivy nanoparticles are essential components in the mucilage exuded by the adventitious roots of English ivy, capable of favoring the generation of strong adhesion strength that aids in surface clinging. The advance in unlocking the molecular mechanisms underlying the ivy-derived adhesive not only forward our understanding of other botanic bioadhesives but may also open new frontiers for the development of ivy-mimetic and ivy-inspired high-strength adhesive composites to eventually expand their engineering applications.

## Materials and Methods

*H. helix* was used for all experiments and was grown as described in refs. 22 and 23. Ivy-derived nanoparticles were isolated and purified as detailed in refs. 21 and 23. DLS and ELS were carried out as described in refs. 82–86. SDS/PAGE and Western blotting analyses were performed according to the procedures outlined in refs. 34 and 87–89. FTIR and XPS were conducted to characterize the purified ivy nanoparticles based on the standard procedures. Monosaccharide composition and linkage analyses and NMR analysis were performed at the Complex Carbohydrate Research Center (CCRC) in the University of Georgia, Athens, GA according to the methods described in ref. 37. Dot blotting test was performed as detailed in ref. 31, with slight modification. ELISA screening test was also performed at the CCRC, using a method as previously described (90). Tensile test was conducted to evaluate the reconstructed ivy-mimetic adhesive composites, according to the standard procedure (ASTM D1002) as previously reported (42, 43, 57–59), with slight modification. More detailed materials and methods are available in *SI Materials and Methods*.

1. Autumn K, et al. (2000) Adhesive force of a single gecko foot-hair. *Nature* 405(6787): 681–685.
2. Geim AK, et al. (2003) Microfabricated adhesive mimicking gecko foot-hair. *Nat Mater* 2(7):461–463.
3. Yu J, et al. (2011) Mussel protein adhesion depends on interprotein thiol-mediated redox modulation. *Nat Chem Biol* 7(9):588–590.
4. Lin Q, et al. (2007) Adhesion mechanisms of the mussel foot proteins mfp-1 and mfp-3. *Proc Natl Acad Sci USA* 104(10):3782–3786.
5. Callow JA, Callow ME (2011) Trends in the development of environmentally friendly fouling-resistant marine coatings. *Nat Commun* 2:244.
6. Sahni V, Blackledge TA, Dhinojwala A (2010) Viscoelastic solids explain spider web stickiness. *Nat Commun* 1:19.
7. Gerbode SJ, Puzey JR, McCormick AG, Mahadevan L (2012) How the cucumber tendril coils and overwinds. *Science* 337(6098):1087–1091.
8. Goriely A, Neukirch S (2006) Mechanics of climbing and attachment in twining plants. *Phys Rev Lett* 97(18):184302.
9. Melzer B, et al. (2010) The attachment strategy of English ivy: A complex mechanism acting on several hierarchical levels. *J R Soc Interface* 7(50):1383–1389.
10. Seidelmann K, Melzer B, Speck T (2012) The complex leaves of the monkey's comb (*Amphilophium crucigerum*, Bignoniaceae): A climbing strategy without glue. *Am J Bot* 99(11):1737–1744.
11. Melzer B, Seidel R, Steinbrecher T, Speck T (2012) Structure, attachment properties, and ecological importance of the attachment system of English ivy (*Hedera helix*). *J Exp Bot* 63(1):191–201.
12. Isnard S, Silk WK (2009) Moving with climbing plants from Charles Darwin's time into the 21st century. *Am J Bot* 96(7):1205–1221.
13. Darwin C (1875) *The Movements and Habits of Climbing Plants* (John Murray, London), p 188.
14. Bowling AJ, Vaughn KC (2008) Structural and immunocytochemical characterization of the adhesive tendril of Virginia creeper (*Parthenocissus quinquefolia* [L.] Planch.). *Protoplasma* 232(3-4):153–163.
15. Groot E, Sweeney E, Rost T (2003) Development of the adhesive pad on climbing fig (*Ficus pumila*) stems from clusters of adventitious roots. *Plant Soil* 248(1-2):85–96.
16. Young RE, et al. (2008) Analysis of the Golgi apparatus in *Arabidopsis* seed coat cells during polarized secretion of pectin-rich mucilage. *Plant Cell* 20(6):1623–1638.
17. Bowling AJ, Vaughn KC (2009) Gelatinous fibers are widespread in coiling tendrils and twining vines. *Am J Bot* 96(4):719–727.
18. Zhang M, Liu M, Prest H, Fischer S (2008) Nanoparticles secreted from ivy rootlets for surface climbing. *Nano Lett* 8(5):1277–1280.
19. Lenaghan SC, Zhang M (2012) Real-time observation of the secretion of a nano-composite adhesive from English ivy (*Hedera helix*). *Plant Sci* 183(0):206–211.
20. Yeston J (2008) Inching up the wall. *Science* 320(5872):23.
21. Lenaghan SC, et al. (2013) Isolation and chemical analysis of nanoparticles from English ivy (*Hedera helix* L.). *J R Soc Interface* 10(87):20130392.
22. Burris JN, Lenaghan SC, Zhang M, Stewart CN (2012) Nanoparticle biofabrication using English ivy (*Hedera helix*). *J Nanobiotechnology* 10(1):41.

23. Huang Y, et al. (2013) Characterization of physicochemical properties of ivy nanoparticles for cosmetic application. *J Nanobiotechnology* 11(1):3.
24. Showalter AM (2001) Arabinogalactan-proteins: Structure, expression and function. *Cell Mol Life Sci* 58(10):1399–1417.
25. Cannon MC, et al. (2008) Self-assembly of the plant cell wall requires an extensin scaffold. *Proc Natl Acad Sci USA* 105(6):2226–2231.
26. Callow JA, Callow ME (2006) The *Ulva* spore adhesive system. *Biological Adhesives*, eds Smith AM, Callow JA (Springer, Heidelberg), pp 63–78.
27. Velasquez SM, et al. (2011) O-glycosylated cell wall proteins are essential in root hair growth. *Science* 332(6036):1401–1403.
28. Seifert GJ, Roberts K (2007) The biology of arabinogalactan proteins. *Annu Rev Plant Biol* 58:137–161.
29. Fincher GB, Stone BA, Clarke AE (1983) Arabinogalactan-proteins: Structure, biosynthesis, and function. *Annu Rev Plant Physiol* 34(1):47–70.
30. Ellis M, Egelund J, Schultz CJ, Bacic A (2010) Arabinogalactan-proteins: Key regulators at the cell surface? *Plant Physiol* 153(2):403–419.
31. Baldwin TC, McCann MC, Roberts K (1993) A novel hydroxyproline-deficient arabinogalactan protein secreted by suspension-cultured cells of *Daucus carota* (purification and partial characterization). *Plant Physiol* 103(1):115–123.
32. Kitazawa K, et al. (2013) β-galactosyl Yariv reagent binds to the β-1,3-galactan of arabinogalactan proteins. *Plant Physiol* 161(3):1117–1126.
33. Sardar HS, Yang J, Showalter AM (2006) Molecular interactions of arabinogalactan proteins with cortical microtubules and F-actin in Bright Yellow-2 tobacco cultured cells. *Plant Physiol* 142(4):1469–1479.
34. Du H, Simpson RJ, Moritz RL, Clarke AE, Bacic A (1994) Isolation of the protein backbone of an arabinogalactan-protein from the styles of *Nicotiana alata* and characterization of a corresponding cDNA. *Plant Cell* 6(11):1643–1653.
35. Poon S, Heath RL, Clarke AE (2012) A chimeric arabinogalactan protein promotes somatic embryogenesis in cotton cell culture. *Plant Physiol* 160(2):684–695.
36. Xu J, Tan L, Goodrum KJ, Kieliszewski MJ (2007) High-yields and extended serum half-life of human interferon α2b expressed in tobacco cells as arabinogalactan-protein fusions. *Biotechnol Bioeng* 97(5):997–1008.
37. Tan L, et al. (2013) An Arabidopsis cell wall proteoglycan consists of pectin and arabinoxylan covalently linked to an arabinogalactan protein. *Plant Cell* 25(1):270–287.
38. Tan L, Qiu F, Lamport DTA, Kieliszewski MJ (2004) Structure of a hydroxyproline (Hyp)-arabinogalactan polysaccharide from repetitive Ala-Hyp expressed in transgenic *Nicotiana tabacum*. *J Biol Chem* 279(13):13156–13165.
39. Comyn J (1997) *Adhesion Science* (Royal Society of Chemistry, London).
40. Ferguson CJ (2000) Core-shell polymers from styrene and vinyl acetate for use as wood adhesives. PhD thesis (Univ of Canterbury, Christchurch, NZ).
41. Damico DJ (2005) *Advances in Adhesives, Adhesion Science, and Testing*, ed Damico DJ (ASTM International, West Conshohocken, PA).
42. Xie D, et al. (2015) Development of injectable citrate-based bioadhesive bone implants. *J Mater Chem B Mater Biol Med* 3(3):387–398.

43. Mehdizadeh M, Weng H, Gyawali D, Tang L, Yang J (2012) Injectable citrate-based mussel-inspired tissue bioadhesives with high wet strength for sutureless wound closure. *Biomaterials* 33(32):7972–7983.
44. Mehdizadeh M, Yang J (2013) Design strategies and applications of tissue bioadhesives. *Macromol Biosci* 13(3):271–288.
45. Zhu Z, Zhai Y, Zhang N, Leng D, Ding P (2013) The development of polycarbophil as a bioadhesive material in pharmacy. *Asian J Pharm Sci* 8(4):218–227.
46. Lee JW, Park JH, Robinson JR (2000) Bioadhesive-based dosage forms: The next generation. *J Pharm Sci* 89(7):850–866.
47. Duncan B, Mera R, Leatherdale D, Taylor M, Musgrove R (2005) Techniques for characterising the wetting, coating and spreading of adhesives on surfaces. NPL Report DEPC-MPR-020 (National Physical Lab, Middlesex, UK).
48. Bowling AJ, Vaughn KC (2008) Immunocytochemical characterization of tension wood: Gelatinous fibers contain more than just cellulose. *Am J Bot* 95(6):655–663.
49. Bowling AJ, Maxwell HB, Vaughn KC (2008) Unusual trichome structure and composition in mericarps of catchweed bedstraw (*Galium aparine*). *Protoplasma* 233(3-4):223–230.
50. Meloche CG, Knox JP, Vaughn KC (2007) A cortical band of gelatinous fibers causes the coiling of redvine tendrils: A model based upon cytochemical and immunocytochemical studies. *Planta* 225(2):485–498.
51. Immerzeel P, Eppink MM, De Vries SC, Schols HA, Voragen AG (2006) Carrot arabinogalactan proteins are interlinked with pectins. *Physiol Plant* 128(1):18–28.
52. O'Neill MA, Ishii T, Albersheim P, Darvill AG (2004) Rhamnogalacturonan II: structure and function of a borate cross-linked cell wall pectic polysaccharide. *Annu Rev Plant Biol* 55:109–139.
53. Demarty M, Morvan C, Thellier M (1984) Calcium and the cell wall. *Plant Cell Environ* 7(6):441–448.
54. Jarvis MC (1984) Structure and properties of pectin gels in plant cell walls. *Plant Cell Environ* 7(3):153–164.
55. Lamport DT, Kieliszewski MJ, Showalter AM (2006) Salt stress upregulates periplasmic arabinogalactan proteins: Using salt stress to analyse AGP function. *New Phytol* 169(3):479–492.
56. Xia L, et al. (2011) Characterization of English ivy (*Hedera helix*) adhesion force and imaging using atomic force microscopy. *J Nanopart Res* 13(3):1029–1037.
57. Rose S, et al. (2014) Nanoparticle solutions as adhesives for gels and biological tissues. *Nature* 505(7483):382–385.
58. Matos-Pérez CR, White JD, Wilker JJ (2012) Polymer composition and substrate influences on the adhesive bonding of a biomimetic, cross-linking polymer. *J Am Chem Soc* 134(22):9498–9505.
59. Zhang H, et al. (2014) Mussel-inspired hyperbranched poly(amino ester) polymer as strong wet tissue adhesive. *Biomaterials* 35(2):711–719.
60. Opanasopit P, Apirakaramwong A, Ngawhirunpat T, Rojanarata T, Ruktanonchai U (2008) Development and characterization of pectinate micro/nanoparticles for gene delivery. *AAPS PharmSciTech* 9(1):67–74.
61. Sila D, et al. (2009) Pectins in processed fruits and vegetables: Part II—Structure–function relationships. *Compr Rev Food Sci Food Saf* 8(2):86–104.
62. Darwin C (1865) On the movements and habits of climbing plants. *J Linn Soc Bot* 9(33–34):1–118.
63. Vaughn KC, Bowling AJ (2011) Biology and physiology of vines. *Hortic Rev* 38:1–21.
64. Crawford BCW, Yanofsky MF (2008) The formation and function of the female reproductive tract in flowering plants. *Curr Biol* 18(20):R972–R978.
65. Crawford BC, Ditta G, Yanofsky MF (2007) The NTT gene is required for transmitting-tract development in carpels of *Arabidopsis thaliana*. *Curr Biol* 17(13):1101–1108.
66. Clarke A, Gleeson P, Harrison S, Knox RB (1979) Pollen-stigma interactions: Identification and characterization of surface components with recognition potential. *Proc Natl Acad Sci USA* 76(7):3358–3362.
67. Lennon KA, Roy S, Hepler PK, Lord EM (1998) The structure of the transmitting tissue of *Arabidopsis thaliana* (L.) and the path of pollen tube growth. *Sex Plant Reprod* 11(1):49–59.
68. Ge X, Chang F, Ma H (2010) Signaling and transcriptional control of reproductive development in *Arabidopsis*. *Curr Biol* 20(22):R988–R997.
69. Lord EM, Mollet J-C (2002) Plant cell adhesion: A bioassay facilitates discovery of the first pectin biosynthetic gene. *Proc Natl Acad Sci USA* 99(25):15843–15845.
70. Monte RW (1976) US Patent 3963655 A.
71. Beachner CE (1968) US Patent 3410704 A.
72. Mollet J-C, Park S-Y, Nothnagel EA, Lord EM (2000) A lily stylar pectin is necessary for pollen tube adhesion to an *in vitro* stylar matrix. *Plant Cell* 12(9):1737–1750.
73. Ferris PJ, et al. (2001) Glycosylated polyproline II rods with kinks as a structural motif in plant hydroxyproline-rich glycoproteins. *Biochemistry* 40(9):2978–2987.
74. Waite JH, Tanzer ML (1981) Polyphenolic substance of *Mytilus edulis*: Novel adhesive containing L-dopa and hydroxyproline. *Science* 212(4498):1038–1040.
75. Budhlall B, Shaffer O, Sudol E, Dimonie V, El-Aasser M (2003) Atomic force microscopy studies of the film surface characteristics of poly (vinyl acetate) latexes prepared with poly (vinyl alcohol). *Langmuir* 19(23):9968–9972.
76. Zhang J, et al. (2008) Effect of annealing on the deformation mechanism of a styrene/n-butyl acrylate copolymer latex film investigated by synchrotron small-angle X-ray scattering. *Macromolecules* 41(12):4353–4357.
77. Chen X, et al. (2011) Structural reorganization of a polymeric latex film during dry sintering at elevated temperatures. *Langmuir* 27(13):8458–8463.
78. Cai HH, Li SD, Tian GR, Wang HB, Wang JH (2003) Reinforcement of natural rubber latex film by ultrafine calcium carbonate. *J Appl Polym Sci* 87(6):982–985.
79. Chen X, Fischer S, Men Y (2011) Temperature and relative humidity dependency of film formation of polymeric latex dispersions. *Langmuir* 27(21):12807–12814.
80. Winnik MA, Yekta A (1997) Associative polymers in aqueous solution. *Curr Opin Colloid Interface Sci* 2(4):424–436.
81. Men Y (2012) Crystallographic deformation in mechanically soft colloidal crystals derived from polymeric latex dispersions. *Soft Matter* 8(21):5723–5727.
82. Kalluri JR, et al. (2009) Use of gold nanoparticles in a simple colorimetric and ultra-sensitive dynamic light scattering assay: Selective detection of arsenic in groundwater. *Angew Chem Int Ed Engl* 48(51):9668–9671.
83. Ipe BI, et al. (2006) Dynamic light-scattering analysis of the electrostatic interaction of hexahistidine-tagged cytochrome P450 enzyme with semiconductor quantum dots. *ChemPhysChem* 7(5):1112–1118.
84. Jans H, Liu X, Austin L, Maes G, Huo Q (2009) Dynamic light scattering as a powerful tool for gold nanoparticle bioconjugation and biomolecular binding studies. *Anal Chem* 81(22):9425–9432.
85. Xu R (2002) Electrophoretic light scattering. *Particle Characterization: Light Scattering Methods*, ed Scarlett B (Springer, Heidelberg), pp 289–343.
86. Berne BJ, Pecora R (2000) *Dynamic Light Scattering: With Applications to Chemistry, Biology, and Physics* (Dover, Mineola, NY).
87. Willats WG, Knox JP (1996) A role for arabinogalactan-proteins in plant cell expansion: Evidence from studies on the interaction of β-glucosyl Yariv reagent with seedlings of *Arabidopsis thaliana*. *Plant J* 9(6):919–925.
88. Schultz CJ, Ferguson KL, Lahnstein J, Bacic A (2004) Post-translational modifications of arabinogalactan-peptides of *Arabidopsis thaliana*. Endoplasmic reticulum and glycosylphosphatidylinositol-anchor signal cleavage sites and hydroxylation of proline. *J Biol Chem* 279(44):45503–45511.
89. Mau SL, et al. (1995) Molecular cloning of cDNAs encoding the protein backbones of arabinogalactan-proteins from the filtrate of suspension-cultured cells of *Pyrus communis* and *Nicotiana alata*. *Plant J* 8(2):269–281.
90. Pattathil S, et al. (2010) A comprehensive toolkit of plant cell wall glycan-directed monoclonal antibodies. *Plant Physiol* 153(2):514–525.
91. Borderies G, et al. (2003) Proteomics of loosely bound cell wall proteins of *Arabidopsis thaliana* cell suspension cultures: A critical analysis. *Electrophoresis* 24(19-20):3421–3432.
92. Debye P, Bueche AM (1948) Intrinsic viscosity, diffusion, and sedimentation rate of polymers in solution. *J Chem Phys* 16(6):573–579.
93. Knox JP, Linstead PJ, King J, Cooper C, Roberts K (1990) Pectin esterification is spatially regulated both within cell walls and between developing tissues of root apices. *Planta* 181(4):512–521.
94. Smallwood M, et al. (1994) Localization of cell wall proteins in relation to the developmental anatomy of the carrot root apex. *Plant J* 5(2):237–246.
95. Knox JP, Linstead PJ, Peart J, Cooper C, Roberts K (1991) Developmentally regulated epitopes of cell surface arabinogalactan proteins and their relation to root tissue pattern formation. *Plant J* 1(3):317–326.
96. Puhlmann J, et al. (1994) Generation of monoclonal antibodies against plant cell-wall polysaccharides. I. Characterization of a monoclonal antibody to a terminal alpha-(1–>2)-linked fucosyl-containing epitope. *Plant Physiol* 104(2):699–710.